Article

Optimal Operation of Isolated Microgrids Considering Frequency Constraints

Josep-Andreu Vidal-Clos [1], Eduard Bullich-Massagué [1], Mònica Aragüés-Peñalba [1], Guillem Vinyals-Canal [1], Cristian Chillón-Antón [1], Eduardo Prieto-Araujo [1], Oriol Gomis-Bellmunt [1], Samuel Galceran-Arellano [1]

[1] Centre d'Innovació Tecnològica en Convertidors Estàtics i Accionaments (CITCEA-UPC), Departament d'Enginyeria Elèctrica, Universitat Politècnica de Catalunya ETS d'Enginyeria Industrial de Barcelona, Avinguda Diagonal, 647, Pl. 2, 08028 Barcelona, Spain

* Correspondence: eduard.bullich@citcea.upc.edu; Tel.: +34 93 405 42 45

Academic Editor: name
Version May 20, 2019 submitted to Appl. Sci.

Abstract: Isolated microgrids must be capable to perform autonomous operation without external grid support. This leads to a challenge when non-dispatchable generators are installed because power unbalances can produce frequency excursions compromising the system operation. This paper addresses the optimal operation of PV-Battery-Diesel based microgrids taking into account the frequency constraints. Particularly, a new stochastic optimization method to maximize the PV generation while ensuring the grid frequency limits is proposed. The optimization problem is formulated including a minimum frequency constraint, which is obtained from a dynamic study considering maximum load and photovoltaic power variations. Once the optimization problem is formulated, 3 complete days are simulated to verify the proper behaviour. Finally, the system is validated in a laboratory scaled microgrid.

Keywords: Energy Management System; microgrids; frequency stability; renewable power generation

---

1. Introduction

The integration of distributed generation requires the development of new concepts for active grid operation, where microgrids are the most promising one [1]. Microgrids are capable to operate in grid connected and in isolated modes [2,3]. In isolated mode, the active power balance to maintain the grid frequency has become one of the main challenges. The integration of large amount of photovoltaic (PV) generation can stress even more the power balance due to the lack of inertia and the fast power variations of the resource. One possible solution to avoid frequency deviations produced by PV power generation is its curtailment [4]. Frequency deviations can also be limited increasing the grid inertia, which can be achieved by connecting rotating machines [5]. The main drawback is that these solutions have and adverse effect on the operation cost.

To solve the power balance problems while minimizing the operation cost, a hierarchical control architecture is commonly used [6–9]. The primary control layer stabilizes the voltage and frequency deviations due to power unbalances by adjusting the active and reactive power references in a time frame of milliseconds. Then, the secondary control is responsible for recovering the voltage and frequency to their reference values. Commonly, it is done by using PI based closed loop controllers in a slower time scale than the primary control response time. And finally, The tertiary control determines the power references to perform the optimal operation of the microgrid.

1.1. Literature review

Different methods has been considered for designing energy management systems (EMS), i.e. the tertiary control layer, for microgrids. These methods mainly consist on i) formulate an objective function; ii) define a set of constraints to ensure the proper system behaviour; and iii) apply an algorithm to find the optimal solution.

In [10], a mixed integer linear program (MILP) is formulated to miniminze the microgrid operation cost. The microgrid includes critical and controllable loads, energy storage, controllable generation and renewable generation. Because of the system under study is connected to the utility grid, any power unbalance is considered to be compensated by the external network producing a very small frequency deviation. Accordingly, power reserves are not considered. Despite the problem formulation does not consider forecast errors, its periodical execution similar to the rolling horizon process permits to redefine periodically the operation plan compensating unpredicted deviations.

The works presented in [11–13] proof the real implementation of different EMSs for the minimum price or minimum cost of the isolated microgrid operation. These papers solve the optimization problems using MILP, multi-layer ant colony optimization and multi-period gravitational search algorithms, respectively. These studies consider perfect forecast. So, the hierarchical control structure is not implemented and power reserves are not considered. As a consequence, power unbalances and frequency deviations are not studied. So, the grid stability cannot be ensured.

The study performed in [14] proposes an heuristic method, based on genetic algorithms, for solving the cost minimization problem for the microgrid operation. It first develop a forecasting method and then formulates the problem and the generic algorithm. The problem formulation differs depending on if the microgrid operates connected or disconected form the main grid, considering load and generation forecast for the power balance equations. As power reserves are considered, the power unbalances due to forecast errors may be compensated, but this may lead to a suboptimal operation point of the microgrid. In addition, the transient response when unbalances due to forecast errors occur is not analysed.

To avoid operating in a suboptimal operation point in microgrids due to foracast errors, different studies propose the formulation of stochastic optimization problems [15–17]. In this method, a set of forecasted scenarios is generated. Then, the decision variables are optimized for all scenarios, where the objective function is the sum of the objective function of each scenario. In the particular case of [15].

In [18], an EMS for minimizing the use of diesel generation in a PV-wind-diesel-battery based isolated microgrid is developed. The optimization problem is formulated as a MILP and executed using the rolling horizon technique to reduce the effects of the uncertainties of forecasted variables. In addition, the primary control layer (particularly the droop curves) vary depending if diesel generation is turned on or off. This fact can affect the transient performance, but a transient study is not performed.

The authors of [11–13] do not consider forecast errors. This issue is solved in [14,18] by considering power reserves. To improve the average optimal operation point against the uncertainty, authors of [15–17] propose a stochastic optimization method. These previous studies does not analyse dynamic and transient behaviour. This gap is treated in [19]. This study develops a multi agent EMS for an isolated microgrid. One of the particularities and not studied in the previous cited papers, is that the transient response considering the primary and secondary control layers is analysed. The tertiary control layer (EMS), which is the objective of the study, determines not only the scheduled setpoints but also the required reserves to compensate photovoltaic and load forecasting errors, avoiding frequency deviations. These frequency deviations are analysed later in a real time dynamic simulator platform.

The frequency deviations is an important aspect that should also be considered. Local controls of generation units will react to these deviations in order to achieve a power balance and to maintain the grid frequency. In [20], the system frequency is introduced into the optimization problem. Particularly, the f-P droop control is considered and a the maximum frequency deviation is constrained. These constraints apply for the steady state, but they do not consider the transient behaviour. An OPF problem which includes the frequency transient behaviour has been presented in [21], explaining the need to limit its deviations. However, the main assumption is that the frequency decrease linearly during the first few seconds until reaching the steady state. The typical frequency transient behaviour usually present and overshoot as shown in [22]. Hence, the maximum frequency deviation during the transient may be greater that the deviation in the steady state. This effect is not considered in [21].

1.2. Required improvements in the EMS development for isolated microgrids

As shown before, EMSs for isolated microgrids are commonly designed without analysing their dynamic behaviour. The primary and secondary control layers are responsible to stabilize the microgrid after disturbance, but the EMS must consider their necessities to perform the operation properly. This issue has been previously solved by incorporating power reserves constraints in the optimization problems of the EMSs [14,19]. Nevertheless, very little dynamic considerations has been performed when designing EMSs. In addition to the power up/down regulation capacity, there are dynamic aspects that should be considered by the EMSs which are not studied yet.

Utility grids are usually characterized by incorporating lots of rotating machines and, consequently, having large inertia. During power unbalances, and until the primary and secondary controls react, the required energy is obtained from the rotating machines leading to frequency variations. Due to the big inertia, these frequency variations are usually small. Accordingly, in grid connected microgrids it can be assumed these deviations are not relevant [10]. In contrast, grid isolated microgrids present low inertia, and even lower when large amount of photovoltaic power is installed. Accordingly these assumptions can no longer be accepted. Power reserves will determine whether the inner control loops will or will not be capable to compensate the microgrid unbalances. But due to the low inertia, the transient frequency deviations can reach unacceptable levels collapsing the system. Despite the study performed in [19] considers the up/down regulation and analyses the dynamic response, the required inertia to ensure the frequency do not exceed the acceptable limit is not studied. Hence, in case the EMS developed in [19] disconnects too match rotating machines, the system stability could be compromised. Similarly, if frequency transients present overshoots, the stability of the system is not ensured by the proposed methods in [20,21].

According to the above issues, for designing a reliable EMS it is still necessary to incorporate dynamic constraints into the problem formulation. Particularly, in addition to the power reserves, the minimum grid inertia to ensure an stable operation should be considered on the tertiary control layer of isolated microgrids.

1.3. Paper contributions

This paper focuses on the above mentioned issue. In particular, an EMS for ensuring that transient frequency deviations do not exceed a defined limit is developed. Accordingly, the main contribution of this paper are:

- The analysis of the parameters that, being available by the EMS, may influence the frequency deviations.
- The formulation of the maximum frequency deviation in front of the maximum power unbalance. This formulation uses the above mentioned parameters.
- The formulation of an EMS including a frequency constraint.
- Validation of the proposed EMS using dynamic simulation and laboratory platform.

Particularly, this paper proposes a power dispatch optimization algorithm for PV-Battery-Diesel based microgrids including demand and PV forecasting. To deal with uncertainty, the problem is based on stochastic optimization and computed on-line, in a similar way than the rolling horizon technique. The algorithm, which maximizes the PV generation, considers a frequency variation constraint obtained by analysing multiple off-line dynamic simulations and performing a statistical study. The result shows that the minimum system frequency depends on the number of connected diesel generators, the battery power generation/consumption and the PV power generation. The algorithm is tested using simulation software (MATLAB-SIMULINK for simulation; and GAMS for solving the MILP optimization problem, using the SCIP solver) and validated in a laboratory platform. Particularly, three different days (based on real second-by-second data) are simulated. Then, one of the simulated days is tested in the laboratory scaled microgrid platform.

2. System description

The system under study is depicted in Figure 1. The microgrid consists of several diesel generators (N_d), where each unit i has a rated power P_{di}; a PV power plant, where the rated power is P_{pv-nom}; a battery which rated power and capacity are $P_{bat-nom}$ and C_{bat} respectively. Finally, all these generation and storage units feed the total power demanded by the loads (P_c). The layout is based on a real stand alone system. It has the particularity that all generation and storage units (controllable units) are connected to the same bus. So, the load side can be treated as a single aggregated load. Each controllable unit has its local controller (LC) which is in charge of managing each resource separately:

- LC for diesel generation power plant: the local controller is in charge of controlling the frequency of the grid. A proportional-integral (PI) controller, where the input is the frequency error (filtered by a low pass filter), computes the mechanical torque setpoint of each diesel generator. This local controller also receives the required number of connected diesel generators and accordingly sends orders of connection/disconnection to each diesel unit. Each diesel generator has its internal controller in charge of reaching the torque setpoint and to perform its connection and disconnection according to the LC requirements. A similar control architecture is found in [23]. The main difference is that in the present paper the PI is a central controller that coordinate all the diesel units, while in [23] a single unit is considered.
- LC for the PV power plant: this LC implements a power-frequency droop curve to provide support to the grid. Reducing the active power will always be possible, but to increase it (under frequency events) will depend on the available active power. The controller is also capable to perform power curtailments. A maximum PV power setpoint is received externally and a PI controller computes the active power setpoint of each PV inverter. This controller is defined in [24], but the ramp rate limitation is not taken into account.
- LC for the battery: this controller receives externally an active power sepoint and applies a power-frequency droop curve to provide grid support. The output is the droop modified setpoint. The inner control loops will be in charge of reaching this value of active power. The dynamic model is simplified as in [25], but the local frequency droop has been included.

3. Methodology

3.1. EMS design requirements

The purpose of this section is to describe the steps followed for designing the EMS. The process is depicted in Figure 2. It shows that the EMS requirements are mainly determined by the characteristics of the system it will operate (System definition), the usage of the forecasting information (System data processing) and the identified operational requirements (System operation requirements).

First, the system characteristics are gathered -mainly the electrical characteristics and the forecasting available data- assuming grid isolated operation. Then, a statistic analysis of the forecasting for PV generation and demand is performed to identify the probability distribution of their errors. This allows to generate random forecast scenarios (as detailed in Section 3.5. Next, the operation for the storage system is defined considering long term variability of PV generation and demand. The minimum number of diesel generating units needed to face the largest demand change expected in the system is also determined. Finally, the EMS is designed, with two main purposes. On the one hand, the optimization problem is formulated based on the steady state equations determining the power

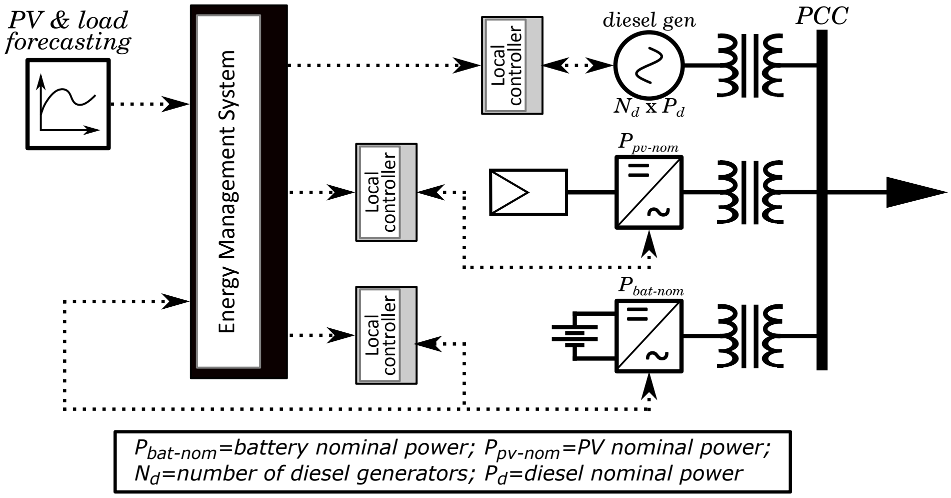

Figure 1. Simplified PV-Battery-Diesel-based microgrid scheme

balances in the system and limiting system variables. On the other hand, a frequency constraint, which will be included in the optimization problem, is formulated (based on dynamic simulation results) relating the PV power generated, the battery power and the number of connected diesels with the minimum allowed frequency after a maximum power unbalance in the system.
The EMS performance is described in Section 3.2. The execution cycle of the EMS is detailed in Section 3.3. The procedure to determine the frequency constraint is explained in Section 3.4. For the stochastic optimization problem it is required to generate a number of random scenarios, which is explained in Section 3.5. Finally, the whole optimization problem formulation is addressed in Section 3.7.

3.2. EMS performance

The objective is to achieve the optimal utilization of the PV energy while achieving a generation-demand balance maintaining the grid frequency. In addition, it ensures that the minimum frequency (f^{mn}) reached after a severe generation-load unbalance is between the limits (see Section 3.4 and the frequency constraint explained later for more detail).

The output variables (the setpoints to the generation and storage units) of the EMS are i) number of diesel generators to be connected (D^*_{con}); ii) the setpoint to the battery (P^*_{bat}); and iii) the maximum PV power setpoint ($P^*_{PV_{max}}$) and are calculated for the remaining of the day at each optimization execution period. On the other hand, the inputs are i) the load forecast (L^c); ii) the available PV power forecast (L^{PV}); and iii) the initial state of charge (SOC). Forecasts include the mean and standard deviation.

Figure 3 shows the time periods used. (T_{for}) represents the time periods when forecasts are updated. (T_{EMS}) is the period between EMS executions. Finally, T_{intra} is the optimization problem time resolution. When the EMS is executed, the output variables (decision variables) are calculated for the rest of the day. While P^*_{bat} and P^*_{PV-max} are calculated with a time resolution of T_{intra}, the resolution of D^*_{con} is T_{EMS}.

3.3. Execution cycle

The optimization algorithm and its execution considers the daily Sun period. So, the horizon of each execution is end of the day. This can be observed in Figure 3, where the execution cycle during the day d is depicted.

EMS period *T* execution: At period $T \in \{1,..,nT_{EMS}\}$ the $P^{bat*}_{T,p}$ & $P^{PV^*_{max}}_{T,p}$ $\forall\ p \in \{1,..,nT_{intra}\}$ are sent to its respective converters. These values are calculated in previous EMS executions (see Figure 3). Then, the SOC at the beginning of the EMS period *T+1* is estimated using the current SOC and the battery setpoints for the current execution period.

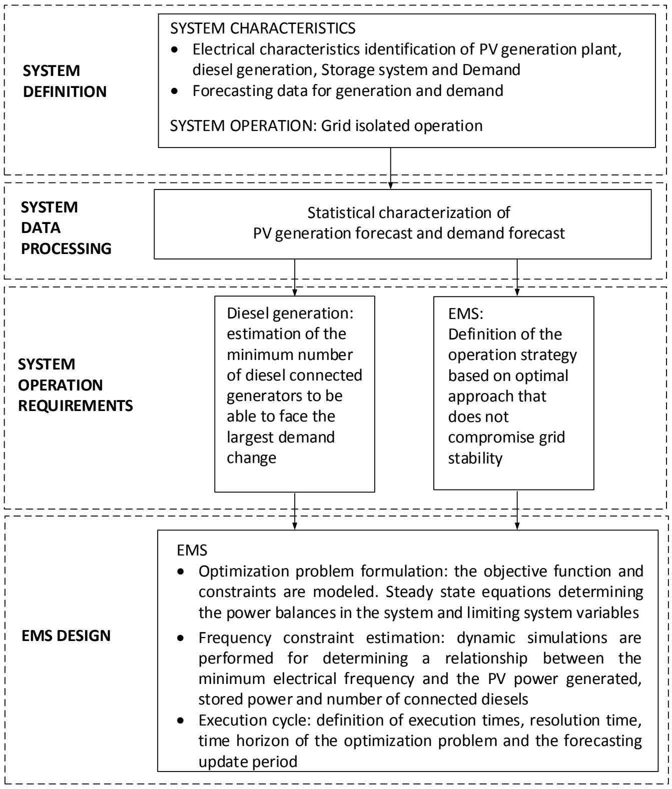

Figure 2. EMS design methodology

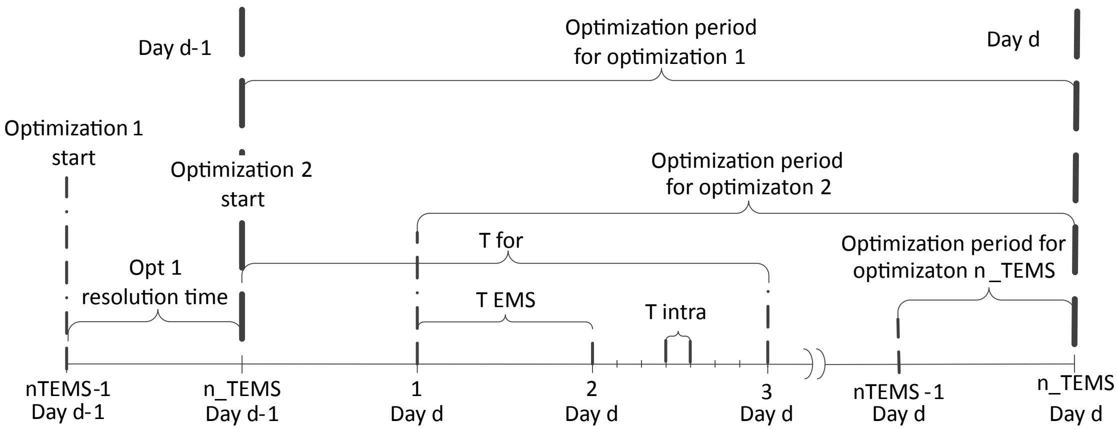

Figure 3. Temporal description of the daily execution cycle

Using the estimated SOC at the EMS period *T+1* and the forecast for the rest of the day d, the optimization problem is solved, and $P_{t,p}^{bat^*}$ & $P_{t,p}^{PV_{max}^*}$ $\forall\ p\ \in \{1, .., nT_{intra}\}$, $\forall t \in \{T+1, .., nT_{EMS}\}$ and $D_t^{con^*}$ $\forall\ t\ \in \{T+1, .., nT_{EMS}\}$ are calculated.

The solution must be reached before the beginning of the EMS period *T+1*. Otherwise, the setpoints calculated for the EMS period *T+1* by the EMS execution at the period *T-1* are sent to the respective converters.

3.4. Modeling frequency deviations

As explained before, one of the requirements of the isolated microgrid is the need to maintain the frequency in the required range. The frequency deviations depend on the grid inertia (i.e. the number of connected rotating machines) among other factors. One possible solution to ensure the frequency requirements is to connect the maximum number of rotating machines (diesel generators) providing large amount of inertia. But these machines usually have a minimum active power generation[1]. So, this strategy leads to a costly (fuel cost) and pollutant (CO_2 emissions) solution. Accordingly, the optimal solution is to connect the minimum number of rotating machines that ensures that, after a maximum power unbalance, the grid frequency will be kept in the required range.

So, the approach of this paper is to obtain an empirical linear equation determining the minimum frequency reached after a maximum power unbalance. This expression will be then used in the optimization algorithm.

To obtain this expression, the worst case is first defined. The load and PV production of a real microgrid have been monitored with 1 second resolution during 6 days and with 30 second resolution during 1 year. Using load data, a maximum load variation of 1.5 MW in 1 second has been identified. This severe variation could have been produced due to the disconnection of a big load. For the case of PV data, it was registered a maximum power variation of 1 MW in 1 second. According to the available recorded data, these changes will not occur simultaneously. So, the worst case considered is that the maximum power unbalance will occur after a sudden load variation of 1.5 MW, representing the situation when the maximum frequency deviation will occur.

Then, a simulation model of the microgrid is created. The model of the diesel generators are described in [23] while simplified PV and battery models are described in [25].

Using the simulation model, a bundle of scenarios varying D_{con} from N_d to N_{dmin} (being N_{dmin} the minimum number of diesel units connected to supply the maximum power unbalance), varying the P^{pv} from the rated PV power to 0 and varying the P^{bat} from P^{mxB} (maximum battery power) to P^{mnB} (minimum battery power) are simulated. In these simulations, the worst case (maximum load variation) is tested and the frequency response is analysed, storing the minimum frequency reached for each simulation. From the analysis, a relation between the EMS output variables and the minimum frequency is performed (this analysis is explained below). In order to maintain the optimization problem solvable using mixed integer linear programming (MILP), a linear regression is proposed for that purpose as (1). Where θ_x are the coefficients of linear regression.

$$f^{mn} = \theta_{ind} + \theta_d \cdot D_{con} + \theta_{pv} \cdot P_{PV} + \theta_{bat} \cdot P_{bat} \tag{1}$$

The minimum frequency reached after the maximum power variation are represented in Figure 4 as a box plot against the ON^{dies}, P^{bat} and $P^{PV_{max}^*}$. For each of the decision variables is possible to observe the tendency of the minimum frequency reached. The lower is the P^{bat} and $P^{PV_{max}^*}$ the higher (in absolute values) is the maximum frequency deviation reached. On the other hand, the lower is the ON^{dies} the lower is maximum frequency deviation reached. Figure 5 shows the summary of

---

[1] Industry has reported that during low load condition diesel engines suffer from the 'slubbering' effect. This effect is related to the low heat in the cylinder, allowing unburned fuel and oil to leak through the slip joints. At the end this lead to power losses, accelerated ageing and high maintenance costs.

performing a linear regression, it can be observed that the coefficients for the $P^{PV^*_{max}}$ and P^{bat} are negative and the coefficient for the ON^{dies} is positive, the p-values for all the coefficients are lower than 10^{-8} and hence the obtained coefficients can be taken as significant.

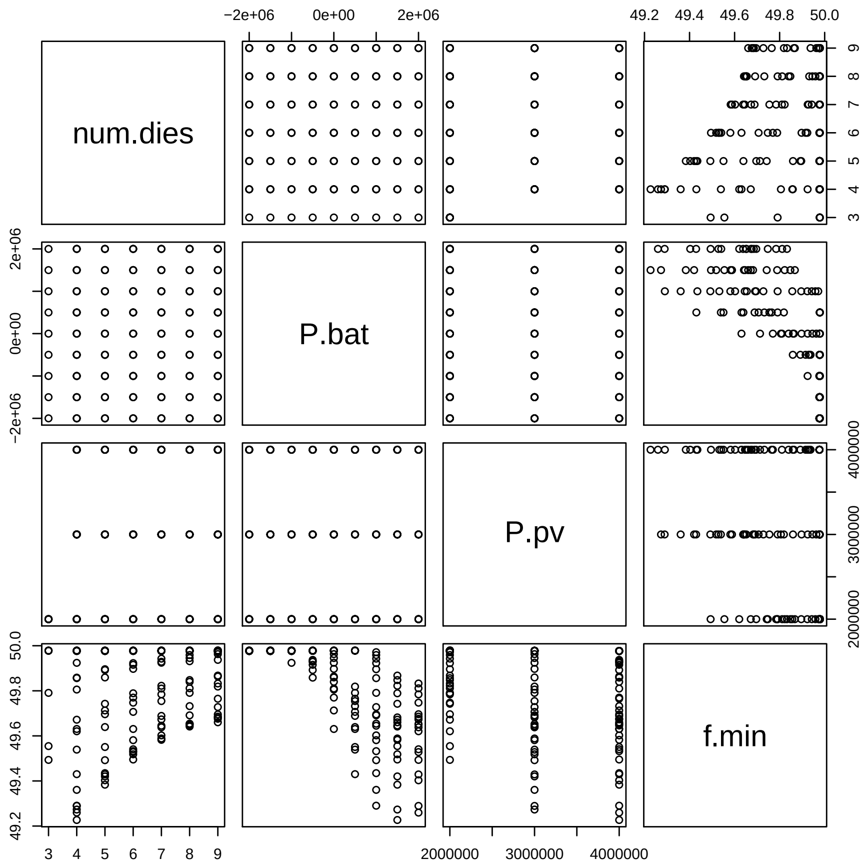

Figure 4. Boxplot showing the relation between the minimum frequency reached and the decision variables of the EMS

```
Coefficients:
              Estimate Std. Error  t value Pr(>|t|)    
(Intercept)  4.991e+01  3.871e-02 1289.562  < 2e-16 ***
num.dies     2.723e-02  4.420e-03    6.160 5.24e-09 ***
P.bat       -1.129e-07  6.247e-09  -18.074  < 2e-16 ***
P.pv.curt   -8.798e-08  9.835e-09   -8.946 6.77e-16 ***
---
Signif. codes:  0 ‘***’ 0.001 ‘**’ 0.01 ‘*’ 0.05 ‘.’ 0.1 ‘ ’ 1

Residual standard error: 0.1055 on 167 degrees of freedom
Multiple R-squared:  0.7218,	Adjusted R-squared:  0.7168 
F-statistic: 144.5 on 3 and 167 DF,  p-value: < 2.2e-16
```

Figure 5. Linear regression results for the coefficients of the minimum frequency equation

3.5. Scenarios generation

The forecasting system updates the forecasts for the rest of the day with a period T_{for}. The forecasts are based on a mean value and an error following a normal distribution with mean value ($\mu_{err} = 0$) and a standard deviation (σ_{err}). Using these values, the EMS generates a number of random scenarios

N_s defined by the the pair $L^{c}_{t,p,s}$ and $L^{PV}_{t,p,s}$, $\forall t \in \{To, ..., n_{TEMS}\}$, $\forall\ p \in \{1, ..., n_{Tintra}\}$; $\forall\ s \in \{1, ..., N_s\}$ being To the actual T^{EMS} period.

3.6. Stochastic formulation approach

The forecast errors are considered by using stochastic formulation. Particularly in this paper, a number of N_s scenarios are generated (more details are given in section 3.5). Then, the decision variables are constant for all scenarios, i.e. devices receive the same setpoints in all scenarios. In contrast, the rest of the variables will be computed depending on each scenario. This way, the optimization problem ensures finding decision variables that fulfils the problem constraints for all scenarios generated. Then, global objective function will be the sum of objective function of each scenario. Note that as more probable is a scenario, more times will be generated and more times will be counted in the global objective function, i.e. the most probable scenarios will present higher weights in the objective function.

3.7. Formulation of the optimization algorithm

The optimization problem is stochastic. It means that from the forecast (mean and deviation values) a number of different scenarios are generated. The solution (the battery setpoints, the maximum PV power setpoints and the number of connected diesel generator setpoints) is unique independently of the scenario, but the constraints must be accomplished for all scenarios. The objective function is the sum of the objective of each scenario. This way we obtain an optimal solution considering forecast errors. In this section, the different optimization sets, decision variables and restrictions required to define the optimization problem are detailed.

3.7.1. Sets

The sets defining the EMS executions and the time resolution are shown in (2) and (3) respectively.

$$T^{EMS} = \{1, ..., n_{TEMS}\} \tag{2}$$

$$T^{intra} = \{1, ..., n_{Tintra}\} \tag{3}$$

Where n_{TEMS} is the number of the remaining executions of the optimization algorithm until the end of the day and n_{Tintra} is the number of periods of T_{intra} s between two executions of the optimization algorithm.

The index of the diesel generators are defined by the set (4), where N_d is the total number of diesel generators.

$$N^{diesel} = \{1, ..., N_d\} \tag{4}$$

It is considered stochastic optimization to take into account forecast errors. Hence, each optimization execution considers N_s scenarios which are generated from the forecast inputs (mean and deviation). The set of the different scenarios is defined in (5).

$$S = \{1, ..., N_s\} \tag{5}$$

3.7.2. Decision variables

The decision variables are those that the optimization algorithm will find in order to to optimize the objective function.

The battery power setpoint is defined as (6), where positive values of power means that the battery is discharging. It is also distinguished if the battery is charging or discharging. The battery charging and discharging powers are defined as (7) and (8) respectively. To prevent obtaining a solution where the battery could simultaneously charge and discharge, a binary variable is defined in (9). The SOC is shown in (10). In the EMS algorithm, it is assumed that the battery setpoint is the same as the real battery power generation/consumption.

$$P_{t,p}^{bat^*},\ \forall\, t \in T^{EMS},\ \forall\, p \in T^{intra} \tag{6}$$

$$P_{t,p}^{bat_{char}},\ \forall\, t \in T^{EMS},\ \forall\, p \in T^{intra} \tag{7}$$

$$P_{t,p}^{bat_{disch}},\ \forall\, t \in T^{EMS},\ \forall\, p \in T^{intra} \tag{8}$$

$$X_{t,p}^{char},\ \forall\, t \in T^{EMS},\ \forall\, p \in T^{intra}; X_{t,p}^{char} \in \{0,1\} \tag{9}$$

$$SOC_{t,p}^{bat},\ \forall\, t \in T^{EMS},\ \forall\, p \in T^{intra} \tag{10}$$

The diesel connection/disconnection setpoint and the power generation of each diesel generator are denoted as (11) and (12) respectively. $ON_{t,p}^{dies}$ is 1 if the diesel generator d at the EMS period t and the intra period d is connected (and 0 otherwise).

$$ON_{t,p}^{dies},\ \forall\, t \in T^{EMS},\ \forall\, d \in N^{Diesel},\ ON_{t,p}^{dies} \in \{0,1\} \tag{11}$$

$$P_{t,p,s,d}^{dies},\ \forall\, d \in N^{Diesel},\ \forall\, s \in S,\ \forall\, t \in T^{EMS},\ \forall\, p \in T^{intra} \tag{12}$$

The PV power generation of each scenario is written as (13), while the maximum PV power setpoint is expressed as (14).

$$P_{t,p,s}^{pv},\ \forall\, s \in S,\ \forall\, t \in T^{EMS},\ \forall\, p \in T^{intra} \tag{13}$$

$$P_{t,p}^{PV_{max}^*},\ \forall\, t \in T^{EMS},\ \forall\, p \in T^{intra} \tag{14}$$

3.7.3. Parameters

The load and PV scenarios are generated according to the forecast mean values and deviations. These scenarios are expressed as (15) and (16) respectively. They represent the active power of load and the available PV power.

$$L_{t,p,s}^{c},\ \forall\, s \in S,\ \forall\, t \in T^{EMS},\ \forall\, p \in T^{intra} \tag{15}$$

$$L_{t,p,s}^{PV},\ \forall\, s \in S,\ \forall\, t \in T^{EMS},\ \forall\, p \in T^{intra} \tag{16}$$

The battery capacity, the initial SOC, the battery efficiency and the maximum and minimum battery active power are written as Cap^{bat}, SOC^{i}, η^{bat}, P^{mxB} and P^{mnB} respectively. The maximum and minimum active power of each diesel unit are expressed as P^{mxD} and P^{mxD} respectively. The minimum frequency is expressed as f^{mn}. The diesel generators performs a frequency control through a PI controller. To provide a power reserve for frequency regulation, a power margin of diesel generators is reserved. This power margin is denoted as $marge_{dies}$.

3.7.4. Objective function

The objective function it to maximize the PV power generation. To do so, the battery will be charged and discharged according to the forecast and the problem requirements. At the charging and discharging process there are some power losses. So, the real useful PV power must take into account them. Accordingly, the objective function is written as (17).

$$[MAX]\, Z = \sum_{t,p,s} P^{PV}_{t,p,s} - n_S\,(1-\eta_{bat})\, abs(P^{bat^*}_{t,p}) \tag{17}$$

To linearise this function, it can be re-written as (18).

$$[MAX]\, Z = \sum_{t,p,s} P^{PV}_{t,p,s} - n_S\,(1-\eta_{bat})\,(P^{bat_{char}}_{t,p} + P^{bat_{disch}}_{t,p}) \tag{18}$$

3.7.5. Constraints

The objective function has been linearized, but to prevent obtaining simultaneous charge and discharge of the battery, the following constrains are included (19)-(23)

$$P^{bat^*}_{t,p} = P^{bat_{char}}_{t,p} - P^{bat_{disch}}_{t,p}\ \forall\, t \in T^{EMS},\ \forall\, p \in T^{intra} \tag{19}$$

$$P^{bat_{char}}_{t,p} \leq P^{mxB} X^{char}_{t,p}\ \forall t \in T^{EMS},\ \forall\, p \in T^{intra} \tag{20}$$

$$P^{bat_{disch}}_{t,p} \leq P^{mxB} (X^{char}_{t,p} - 1)\ \forall\, t \in T^{EMS},\ \forall\, p \in T^{intra} \tag{21}$$

$$P^{bat_{char}}_{t,p} \geq 0\ \forall\, t \in T^{EMS},\ \forall\, p \in T^{intra} \tag{22}$$

$$P^{bat_{disch}}_{t,p} \geq 0\ \forall\, t \in T^{EMS},\ \forall\, p \in T^{intra} \tag{23}$$

Then, the power balance at each period must be accomplished. This is forced by the restriction (24).

$$P^{pv}_{t,p,s} + \sum_{d \in N^{Diesel}} P^{dies}_{t,p,s,d} + P^{bat^*}_{t,p} - L^{c}_{t,p,s} = 0 \forall\, t \in T^{EMS},\ \forall\, p \in T^{intra},\ \forall\, s \in S \tag{24}$$

Then, as commented before, a margin of diesel generation is reserved for frequency regulation. So, the maximum diesel generation is limited (equation (25))

$$\sum_{d \in N^{Diesel}} P^{dies}_{t,p,s,d} \leq \sum_{d \in N^{Diesel}} ON^{dies}_{t,d} P^{mxD} - marge_{dies} \forall\, t \in T^{EMS},\ \forall\, p \in T^{intra},\ \forall\, s \in S \tag{25}$$

The relationship between the SOC at the instant t and the SOC at the instant $t-1$ is shown in (26). The SOC is between 0 and 1 p.u. This constraint is formulated as (27). On the other hand, the battery power limits constraint is (28).

$$\begin{aligned}
&\text{-If } T^{EMS} = 1 \text{ and } T^{intra} = 1\\
&SOC^{bat}_{t,p} = SOC^{initial} - P^{bat}_{t,p} \frac{\Delta t}{Cap^{bat}}\ \forall\, t \in T^{EMS},\ \forall\, p \in T^{intra}\\
&\text{-If } T^{EMS} \geq 1 \text{ and } T^{intra} = 1\\
&SOC^{bat}_{t,p} = SOC^{bat}_{t-1,|p|} - P^{bat}_{t,p} \frac{\Delta t}{Cap^{bat}}\ \forall\, t \in T^{EMS},\ \forall\, p \in T^{intra}\\
&\text{-If } T^{intra} \neq 1\\
&SOC^{bat}_{t,p} = SOC^{bat}_{t,p-1} - P^{bat}_{t,p} \frac{\Delta t}{Cap^{bat}}\ \forall\, t \in T^{EMS},\ \forall\, p \in T^{intra}
\end{aligned} \tag{26}$$

$$0 \leq SOC^{bat}_{t,p} \leq 1\ \forall\, t \in T^{EMS},\ \forall\, p \in T^{intra} \tag{27}$$

$$P^{mnB} \leq P^{bat}_{t,p} \leq P^{mxB}\ \forall\ t \in T^{EMS},\ \forall\ p \in T^{intra} \tag{28}$$

Then, the PV power cannot be greater than the available PV power of the corresponding scenario. So, equation (29) must be included into de optimization algorithm. The PV power must be also lower than the maximum PV power setpoint (30).

$$P^{PV}_{t,p,s} \leq L^{PV}_{t,p,s}\ \forall\ t \in T^{EMS},\ \forall\ p \in T^{intra},\ \forall\ s \in S \tag{29}$$

$$P^{PV}_{t,p,s} \leq P^{PV^*_{max}}_{t,p}\ \forall\ t \in T^{EMS},\ \forall\ p \in T^{intra},\ \forall\ s \in S \tag{30}$$

Each diesel unit has a maximum and a minimum power at each scenario, which is formulated as (31).

$$ON^{dies}_{d,t,s} P^{mnD}_{d} \leq P^{dies}_{t,p,s} \leq P^{mxD} ON^{dies}_{d,t,s} \forall\ t \in T^{EMS}, \forall\ p \in T^{intra},\ \forall\ s \in S \tag{31}$$

Finally, the minimum frequency constraint is included in the optimization model. In the previous section, it has been shown how to express the minimum frequency reached in the microgrid after a maximum power unbalance. This constraint is written as (32).

$$f^{mn} \leq \theta_{ind} + \theta_d \sum_d ON^{dies}_{t,d} + \theta_{bat} P^{bat^*}_{t,p} + \theta_{pv} P^{PV^*_{max}}_{t,p} \forall\ t \in T^{EMS},\ \forall\ p \in T^{intra} \tag{32}$$

4. Case study

Based on a real case, the microgrid includes: 9x1.2 MVA diesel units, 2x560 kWh batteries, that are interconnected through 4x550 kVA inverters (2 inverters per battery). The total battery power is then 2.2 MVA. The rated power of the PV plant is 10 MW, similar to the one presented in [24]. The minimum accepted frequency is $f^{mn} = 49.0$ Hz. Finally, Table 1 shows the problem parameters.

Table 1. Parameters for the EMS optimization problem

Parameter	Value	Parameter	Value	Parameter	Value
n_{TEMS}	288	Cap^{bat}	1120 kWh	P^{mnB}	-2200 kW
n_{Tintra}	10	SOC^i	0.9	P^{mnD}	0.3*1100 kW
N_d	9	η^{bat}	0.9	P^{mxD}	1100 kW
N_s	5	P^{mxB}	2200 kW	$marge_{dies}$	2000 kW

Three scenarios have been simulated. The load consumption is the same for all scenarios and shown in the result plots. The difference between the three scenarios is reflected in the available PV power profile. In the first case, after 12:30 pm., the available PV profile presents large variations. The second scenario has lower PV variability, but it is not a full sunny day. Finally, the last case consists of a sunny day with not appreciable fast PV power variations. The simulation results are shown in Figure 6 for the first case, in Figure 7 for the second case and in Figure 8 for the last case. Note that the simulation has considered the execution cycle explained in Section 3.3 and the EMS outputs are introduced to the dynamic model.

For each scenario, the top plot depicts the active power of microgrid's devices as well as the power demand and the available PV power. In the middle plot, the SOC and the connections of diesel units can observed. Then, the bottom plot shows the frequency response of the microgrid, being the green lines the frequency droop dead-band (our of this range, the PV plant and the batteries provide frequency support). It can be observed that for the three scenarios, the battery is discharged at the beginning of the day in order to be able to charge during the hours of high PV power. Also, as it could be expected, the active power of diesel generators and the connected units follows a trend complementary to the PV power generation. So, during the peak PV production hours the amount of connected diesel generators is lower, as well as their production. It is also shown that the frequency deviations are kept inside the acceptable range. Comparing the total PV energy generated to the available PV energy for the three scenarios, the relative amount of used PV energy has been 94.57 %, 84.46 % and 94.98 % respectively. The second scenario has the lower PV profitability, but note that in this case, the maximum available PV power is higher than the load in some periods.

Between the times 13h-15h, the frequency exceed the droop dead-band several times. So, the PV and battery provide frequency support. This happens because during this period the number of connected diesel generators is small (low inertia). Hence, either the large PV fluctuations or the connection of new generators injecting active power produce a frequency transient. While the frequency may exceed the frequency droop dead-band (green lines), it does not exceed the minimum value of 49 Hz.

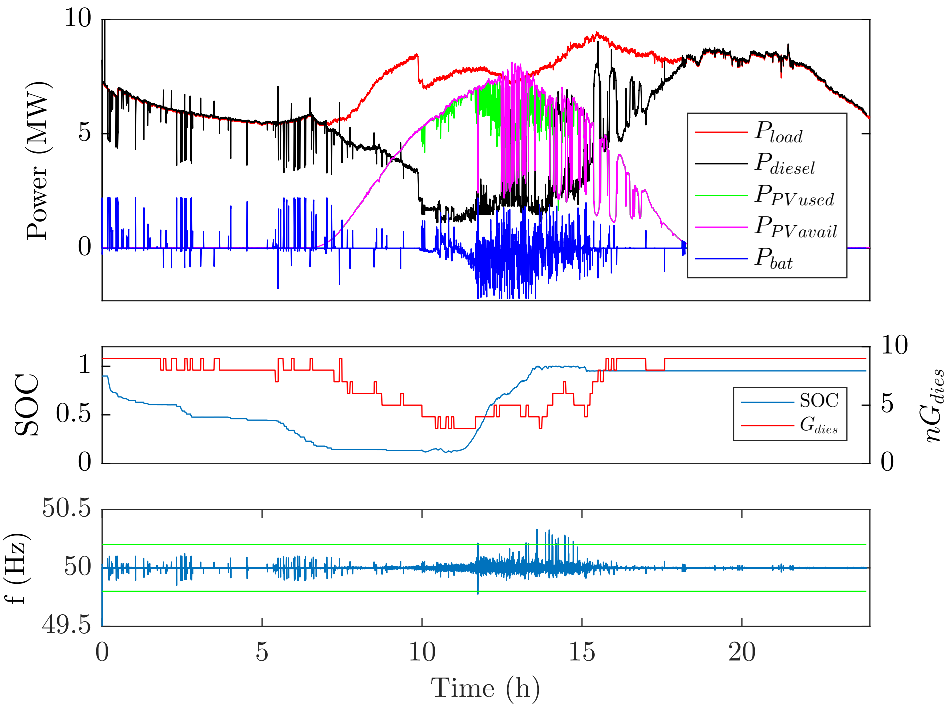

Figure 6. Simulation results for the first scenario (high PV power variability after the midday)

5. Experimental validation

5.1. Platform description

An emulated microgrid has been used for performing the experimental emulation. As described in [26], an emulator consists on a platform capable to convert software processed variables to real magnitudes. Accordingly, real equipment can be tested by its interconnection to the emulator platform. Hence, the system presented above can be tested properly through the emulation concept.

The layout of the laboratory microgrid (emulated microgrid) and its physical devices are depicted in Figures 9(a) and 9(b), respectively. The emulated devices (diesel units, PV generators, storage, and loads) mimic the behaviour of the real device they are representing and form the emulated subsystem of the experimental setup. They are configured using a dedicated PC and a communication network. On the other hand, the real devices of the experimental setup are the PV and battery inverters, the power transformers, the EMS (which is implemented in a dedicated PC) as well as the communication

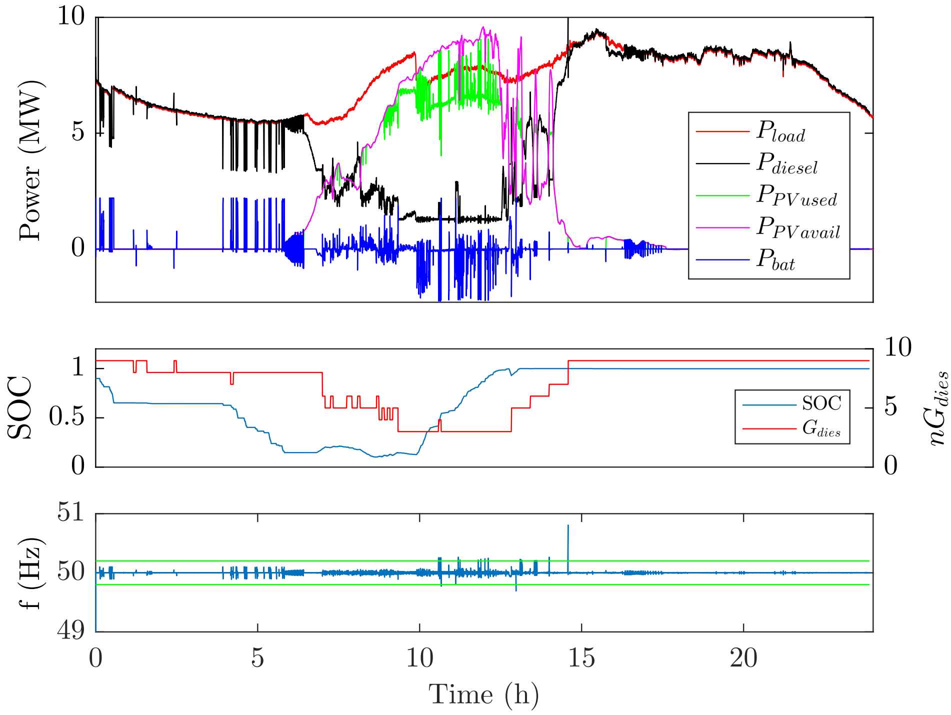

Figure 7. Simulation results for the second scenario (medium PV variability)

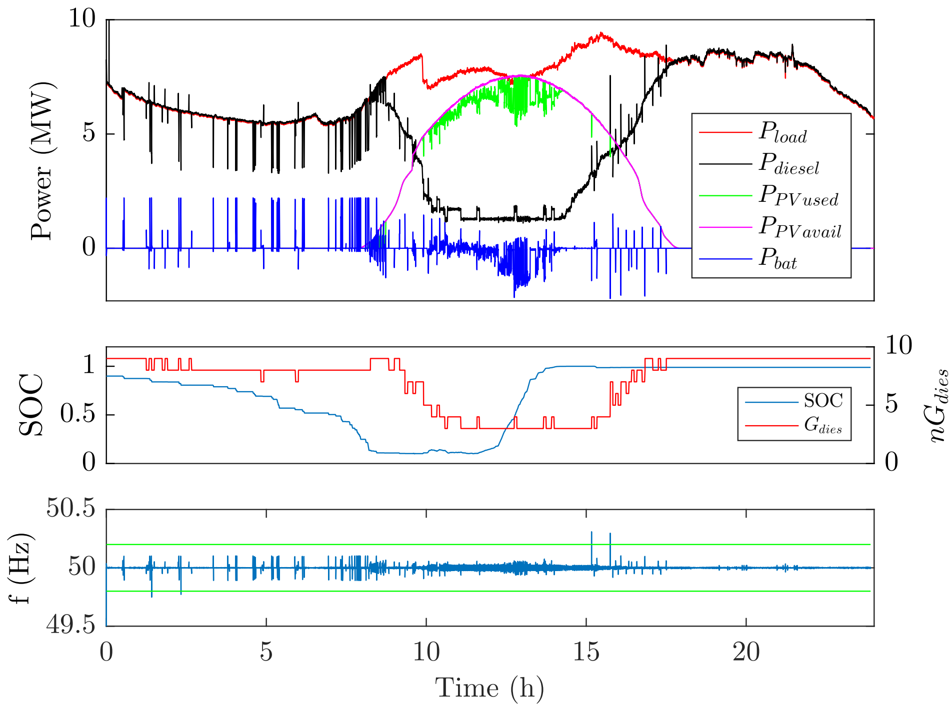

Figure 8. Simulation results for the third scenario (low PV variability)

network and the SCADA system. Because it is desired to emulate the isolated operation, the switch interconnecting the real system with the external grid is opened.

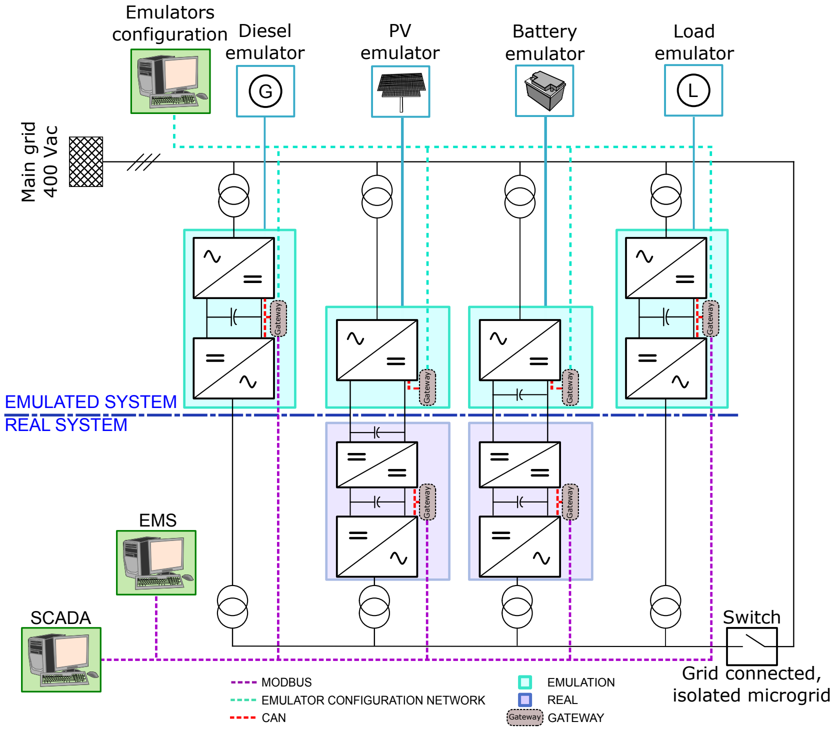

(a) Microgrid emulator scheme

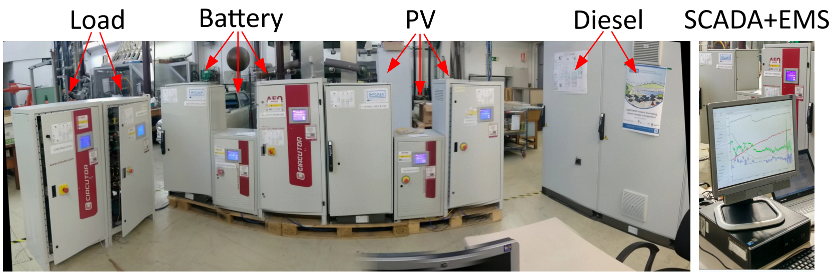

(b) Microgrid photo

Figure 9. Microgrid description

5.2. Emulation results

The simulated results are validated using the first test case (the one presenting the highest PV power variability) and the emulation platform under a real time emulation test. The input data has been scaled-down according the emulators power ratings. The outputs of the EMS are sent, periodically (T_{EMS} =5 minutes), to the devices (emulated). In Figure 10, the experimental results can be observed, showing how the response is very similar to the simulation results. In particularly, it can be observed the same tendency in the diesel units connections and disconnections as well as in the battery utilization. An important observation is that generally, the generation is greater than the load. It is due to the fact that the emulators inverters has power losses.

6. Conclusion

A new methodology for the optimal operation of isolated microgrids has been proposed. This methodology is based on stochastic optimization in order to consider the forecast errors. In addition, a

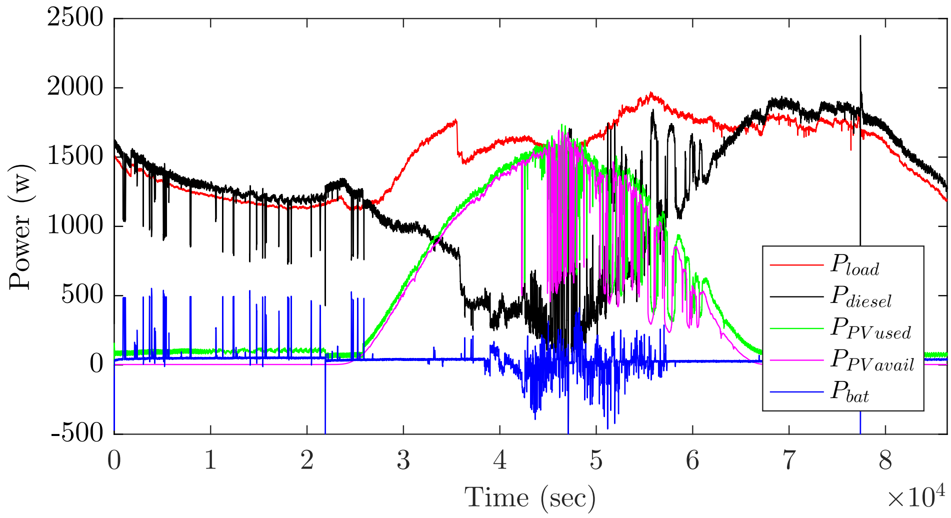

Figure 10. Laboratory emulation results for the first scenario (high PV power variability after the midday

minimum frequency constraint has been formulated and included to the optimization algorithm to ensure the secure operation of the microgrid. To maintain the optimization problem as a mixed integer linear problem, this constraint has been defined using a linear regression.

Three different scenarios, based on real data, have been tested using a dynamic model of the microgrid. The results show a good behaviour with a stable grid frequency and high rate of PV energy used.

After proving the proper response of the EMS using a simulation model, it has been implemented to manage a laboratory scale microgrid, where real time limitations, communication delays and measurement errors occur. It has been shown that the system can also operate properly with real platforms having similar behaviour to the simulated system.

7. Aknowledgements

The research leading to these results has received support of the Secretaria d'Universitats i Recerca del Departament d'Economia i Coneixement de la Generalitat de Catalunya and Serra Hunter Programme.

The authors would like to thank Luis Serrano and Carlos Pacheco from GreenPowerMonitor for their support in this work.

References

1. Aegerl, C.S.; Tao, L., The Microgrids Concept. In *Microgrids Architectures and Control*; Hatziargyriou, N., Ed.; John Wiley and Sons, 2013.
2. DOE. Summary Report: 2012 DOE Microgrid Workshop, 2012.
3. Bullich-Massagué, E.; Díaz-González, F.; Aragüés-Peñalba, M.; Girbau-Llistuella, F.; Olivella-Rosell, P.; Sumper, A. Microgrid clustering architectures. *Applied Energy* **2018**, *212*, 340 – 361.
4. Neely, J.; Johnson, J.; Delhotal, J.; Gonzalez, S.; Lave, M. Evaluation of PV frequency-watt function for fast frequency reserves. 2016 IEEE Applied Power Electronics Conference and Exposition (APEC), 2016, pp. 1926–1933.
5. Kundur, P.; Balu, N.; Lauby, M. *Power system stability and control*; EPRI power system engineering series, McGraw-Hill, 1994.
6. Martin-Martínez, F.; Sánchez-Miralles, A.; Rivier, M. A literature review of Microgrids: A functional layer based classification. *Renewable and Sustainable Energy Reviews* **2016**, *62*, 1133 – 1153.

7. Han, Y.; Shen, P.; Zhao, X.; Guerrero, J.M. Control Strategies for Islanded Microgrid Using Enhanced Hierarchical Control Structure With Multiple Current-Loop Damping Schemes. *IEEE Transactions on Smart Grid* **2017**, *8*, 1139–1153.
8. Vandoorn, T.L.; Vasquez, J.C.; Kooning, J.D.; Guerrero, J.M.; Vandevelde, L. Microgrids: Hierarchical Control and an Overview of the Control and Reserve Management Strategies. *IEEE Industrial Electronics Magazine* **2013**, *7*, 42–55.
9. Bidram, A.; Davoudi, A. Hierarchical Structure of Microgrids Control System. *IEEE Transactions on Smart Grid* **2012**, *3*, 1963–1976.
10. Parisio, A.; Rikos, E.; Glielmo, L. A Model Predictive Control Approach to Microgrid Operation Optimization. *IEEE Transactions on Control Systems Technology* **2014**, *22*, 1813–1827.
11. Marzband, M.; Sumper, A.; Domínguez-García, J.L.; Gumara-Ferret, R. Experimental validation of a real time energy management system for microgrids in islanded mode using a local day ahead electricity market and MINLP. *Energy Conversion and Management* **2013**, *76*, 314 – 322.
12. Marzband, M.; Yousefnejad, E.; Sumper, A.; Domínguez-García, J.L. Real time experimental implementation of optimum energy management system in standalone Microgrid by using multi layer ant colony optimization. *International Journal of Electrical Power and Energy Systems* **2016**, *75*, 265 – 274.
13. Marzband, M.; Ghadimi, M.; Sumper, A.; Domínguez-García, J.L. Experimental validation of a real-time energy management system using multi period gravitational search algorithm for microgrids in islanded mode. *Applied Energy* **2014**, *128*, 164 – 174.
14. Chen, C.; Duan, S.; Cai, T.; Liu, B.; Hu, G. Smart energy management system for optimal microgrid economic operation. *IET Renewable Power Generation* **2011**, *5*, 258–267.
15. Sobu, A.; Wu, G. Optimal operation planning method for isolated micro grid considering uncertainties of renewable power generations and load demand. IEEE PES Innovative Smart Grid Technologies, 2012, pp. 1–6.
16. Lazaroiu, G.C.; Dumbrava, V.; Balaban, G.; Longo, M.; Zaninelli, D. Stochastic optimization of microgrids with renewable and storage energy systems. 2016 IEEE 16th International Conference on Environment and Electrical Engineering (EEEIC), 2016, pp. 1–5.
17. Cau, G.; Cocco, D.; Petrollese, M.; Kær, S.K.; Milan, C. Energy management strategy based on short-term generation scheduling for a renewable microgrid using a hydrogen storage system. *Energy Conversion and Management* **2014**, *87*, 820 – 831.
18. Palma-Behnke, R.; Benavides, C.; Lanas, F.; Severino, B.; Reyes, L.; Llanos, J.; Sáez, D. A Microgrid Energy Management System Based on the Rolling Horizon Strategy. *IEEE Transactions on Smart Grid* **2013**, *4*, 996–1006.
19. Zhao, B.; Xue, M.; Zhang, X.; Wang, C.; Zhao, J. An {MAS} based energy management system for a stand-alone microgrid at high altitude. *Applied Energy* **2015**, *143*, 251 – 261.
20. Sanseverino, E.R.; Nguyen, N.Q.; Silvestre, M.L.D.; Zizzo, G.; de Bosio, F.; Tran, Q.T.T. Frequency constrained optimal power flow based on glow-worm swarm optimization in islanded microgrids. 2015 AEIT International Annual Conference (AEIT), 2015, pp. 1–6.
21. Zhang, G.; McCalley, J. Optimal power flow with primary and secondary frequency constraint. 2014 North American Power Symposium (NAPS), 2014, pp. 1–6.
22. Díaz-González, F.; Hau, M.; Sumper, A.; Gomis-Bellmunt, O. Participation of wind power plants in system frequency control: Review of grid code requirements and control methods. *Renewable and Sustainable Energy Reviews* **2014**, *34*, 551 – 564.
23. Theubou, T.; Wamkeue, R.; Kamwa, I. Dynamic model of diesel generator set for hybrid wind-diesel small grids applications. 2012 25th IEEE Canadian Conference on Electrical and Computer Engineering (CCECE), 2012, pp. 1–4.
24. Bullich-Massagué, E.; Ferrer-San-José, R.; Aragüés-Peñalba, M.; Serrano-Salamanca, L.; Pacheco-Navas, C.; Gomis-Bellmunt, O. Power plant control in large-scale photovoltaic plants: design, implementation and validation in a 9.4 MW photovoltaic plant. *IET Renewable Power Generation* **2016**, *10*, 50–62.
25. Bullich-Massagué, E.; Aragüés-Peñalba, M.; Sumper, A.; Boix-Aragones, O. Active power control in a hybrid PV-storage power plant for frequency support. *Solar Energy* **2017**, *144*, 49 – 62.
26. Prieto-Araujo, E.; Olivella-Rosell, P.; Cheah-Mañe, M.; Villafafila-Robles, R.; Gomis-Bellmunt, O. Renewable energy emulation concepts for microgrids. *Renewable and Sustainable Energy Reviews* **2015**, *50*, 325 – 345.